EXTRACTION OF VELOCITY FIELDS FOR GEOPHYSICAL FLUIDS FROM A SEQUENCE OF IMAGES

Didier Auroux

Institut de Mathématiques de Toulouse
Université Paul Sabatier Toulouse 3
31062 Toulouse cedex 9, France
auroux@math.univ-toulouse.fr

ABSTRACT

We consider the assimilation of satellite images, within the framework of data assimilation in geophysical systems. Based on the constant brightness assumption, we define a nonlinear functional measuring the difference between two consecutive images, the first one being transported to the second one by the unknown velocity. By considering a multiscale approach and a Gauss-Newton minimization algorithm, we can estimate the entire velocity fields at a high frame rate and then assimilate these pseudo-observations.

Index Terms— Velocity estimation, variational approach, nonlinear minimization, constant brightness assumption, multiscale algorithm.

1. INTRODUCTION

Estimating the motion of a fluid is of great interest, particularly in geophysics where the fluid can be the ocean. Applications of the motion estimation in this domain include the assimilation of images data in oceanographic models, and a possible improvement of the forecasts.

The idea of this paper is to define a fast and efficient way to identify, or extract, velocity fields from several images (or a complete sequence of images). Assuming this point, we would then be able to obtain billions of pseudo-observations, corresponding to the extracted velocity fields, that could be considered in the usual data assimilation processes.

The hypothesis that is underlying this work is that the grey level of the points are preserved during the motion, this is known as the constant brightness hypothesis. The constant brightness hypothesis was introduced in [1], and the linearized equation derived from this hypothesis is the cornerstone of optical flow methods [2, 3, 4].

This hypothesis is justified here in the framework of oceanography, as the objet of interest, allowing us to track the fluid and identify its velocity, is usually a passive tracer, at least on relative short time periods: chlorophyll, sea surface temperature, chemical pollutants (e.g. hydrocarbons)... All these tracers do not interact with the water on a short time period, and they are passively transported by the fluid.

We propose here to use an integrated version of the constant brightness hypothesis. Instead of linearizing the constant brightness hypothesis like in standard optical flow techniques, we define a nonlinear cost function that takes into account the fact that time sampling occurs at a finite rate. Moreover, the combination of bilinear interpolation of gray-levels with spatial regularization provides an accurate estimation of sub-pixel motion.

The cost function obtained from the integrated constant brightness assumption is minimized in nested subspaces of admissible displacement vector fields. The vector fields that we consider are piecewise linear with respect to each space variable, on squares defined by a grid. This grid is iteratively refined, and at each level the optimal displacement field is estimated rapidly since the Jacobian of the cost function is assembled using a finite-element method (only one reading of the data is required).

2. DESCRIPTION OF THE ALGORITHM

2.1. Nonlinear cost function

The velocity estimation relies on the following hypothesis: the brightness of the points does not change between successive frames (at least when the time step between successive images is small enough). Let Ω denote the rectangular domain where the images are defined. The motion between the instants t_0 and t_1 where the images are I_0 and I_1 is then the vector field (u, v) such that for every point $(x, y) \in \Omega$,

$$I_1(x + u(x, y), y + v(x, y)) = I_0(x, y). \tag{1}$$

A vector field satisfying equation (1) is not unique, this is known as the aperture problem in optical flow.

Denote $\mathcal{L}$ the set of Lipschitz vector fields. Consider the following function:

$$F(I_0, I_1; u, v)(x, y) = I_1(x+u(x, y), y+v(x, y))-I_0(x, y), \tag{2}$$

where the vector field $(u, v) \in \mathcal{L}$ and the images I_0 and I_1 are continuously differentiable.

The map F is differentiable with respect to (u, v), and for $(u, v) \in \mathcal{L}$ and $\mathbf{d} = (du, dv) \in \mathcal{L}$,

$$DF(u, v).\mathbf{d}(x, y) = \nabla I_1(x + u(x, y), y + v(x, y)).\mathbf{d}(x, y).$$

The optimal displacement vector field between the images I_0 and I_1 minimizes the following cost-function:

$$J(u, v) = \frac{1}{2} \int_\Omega \left[F(I_0, I_1; u, v)(x, y)\right]^2 \, dx \, dy + \frac{1}{2}\alpha R(u, v), \tag{3}$$

where $R(u, v)$ is a spatial regularization term and α is the regularization factor.

The minimum of J is estimated in a nested sequence of subspaces of $\mathcal{L}$. On a small dimensional subspace, the optimization is efficient and the algorithm is not trapped in local minima. The result is used as initial guess to minimize J in a larger subspace.

2.2. Regularization

Various regularization terms were used in our numerical experiments. In these definitions, $\| \, . \, \|$ represents the L^2 norm of a scalar or vector field on the image. We only detail the main regularizations, that provided the best results.

$$\begin{aligned} R_0(u, v) &= \|u\|^2 + \|v\|^2, & (4)\\ R_1(u, v) &= \|\nabla u\|^2 + \|\nabla v\|^2 = \|\partial_x u\|^2 + \|\partial_y u\|^2 & (5)\\ &+ \|\partial_x v\|^2 + \|\partial_x v\|^2, & (6)\\ R_{div}(u, v) &= \|div(u, v)\|^2 = \|\partial_x u + \partial_y v\|^2, \end{aligned}$$

In all the cases, the regularization term is the square of the image of (u, v) by a linear operator S. Below, the unifying following notation is used:

$$R(u, v) = ||S(u, v)||^2.$$

where S is a linear operator. Some scalar coefficients have also been considered in order to weight the different terms of a given regularization.

2.3. Multiscale approach and optimization

The minimization of the cost-function J is performed in nested subspaces:

$$\mathcal{C}_{16} \subset \mathcal{C}_8 \subset \mathcal{C}_4 \subset \mathcal{C}_2 \subset \mathcal{C}_1,$$

where the set $\mathcal{C}_q$ of admissible displacement fields at the scale q contains piecewise affine vector fields with respect to each space variable, on squares of size $q \times q$ pixels. We present and adapt here the method that was introduced in [5]. The difference with hierarchical techniques issued from the optical flow family (e.g. [6, 7, 8, 9]) is that we do not linearize the cost function. This should help to find large displacements, where the domain of linearity of the luminance function is not valid. Another innovation of the present work is the efficient computation of the product $DF^T DF$ of the Jacobian of the first term of the cost function (3) by its transpose. This efficient computation comes from the observation that this matrix is sparse and can be assembled like a finite-element matrix using one loop over the data.

The space $\mathcal{C}_{16}$ is typically of small dimension, hence the minimization of J on C_{16} is fast and robust when a zero vector field is used as initial guess. The optimal vector field obtained at a given scale in the space $\mathcal{C}_q$ is used as initial guess to find the minimum at the finer scale in the space $\mathcal{C}_{q/2}$.

The optimization of the nonlinear cost function J on $\mathcal{C}_q$ is performed by Gauss-Newton's method. When an initial guess (u^0, v^0) is given, the k-th iteration reads

$$(u^k, v^k) := (u^{k-1}, v^{k-1}) + (du^k, dv^k),$$

where (du^k, dv^k) solves

$$(DF^T DF + \alpha S^T S)(du, dv) = -DF^T F - \alpha S^T S(u, v), \tag{7}$$

where $F = F(I_0, I_1; u^{k-1}, v^{k-1})$ is the error, $DF = DF(I_0, I_1; u^{k-1}, v^{k-1})$ is the Jacobian matrix of the error, and S is the linear operator associated to the regularization term.

3. NUMERICAL RESULTS ON EXPERIMENTAL DATA

We consider data extracted from several experiments on the Coriolis rotating platform [10]. A large rotating turntable (diameter: 13 meters) allows us to reproduce the oceanic or atmospheric flows. Some particles are inserted in the water as the platform rotates, and among the various measurement devices, a camera takes pictures of the experiment [11].

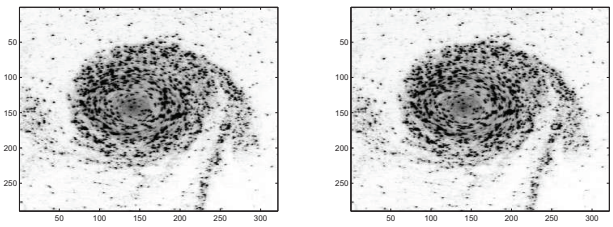

Fig. 1. Concentration images I_0 and I_1 at time steps 28 and 29 respectively.

Figure 1 shows two images extracted from this other experimental movie. The structure of the velocity is the same as in the previous subsection: a vortex in a global translation displacement. The multiscale approach of our algorithm is used (see previous sections), looking first for a piecewise

affine velocity field every 16×16 pixels, and then refining 4 times the mesh. The number of iterations is 50 on the coarse grid, and 1 on the finest grid. For each intermediate mesh, the minimization process is stopped when the decreasing rate of the cost function is lower than a threshold.

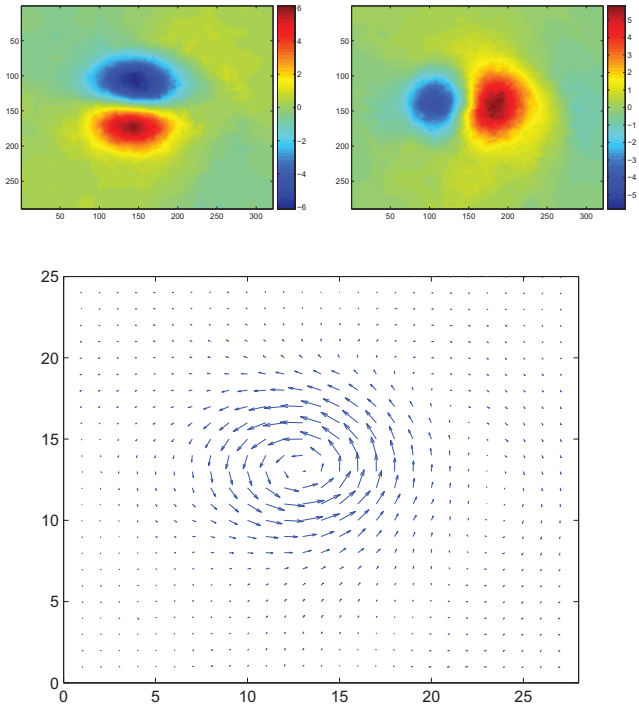

Fig. 2. Identified velocity between images I_0 and I_1: longitudinal (left) and transversal (right) components on the top, velocity field on the bottom.

Figure 2 shows the identified velocity components and field, using this multiscale approach. The velocity field is represented every 12 pixels for visualization reasons. The identified velocity is quite smooth, even though the regularization coefficient is the same as in the previous experimental results. Here, it is very easy to see the global structure of the velocity field, with a characteristic counterclockwise rotating vortex, nearly located in the middle of the image. The global displacement of the structure is a small translation to the top, as the mean of the longitudinal components is nearly zero whereas the mean of the transversal component of the velocity is slightly positive.

Figure 3 shows the results of the identification process. On the left is represented the difference between the two original images, and on the right, the difference between the second image and the first one being transported by the identified velocity. Even if the original difference looks quite big, with a lot of small displacements everywhere, one can see that the smooth identified velocity provides a very good transport between these two images, as the difference has been drastically reduced.

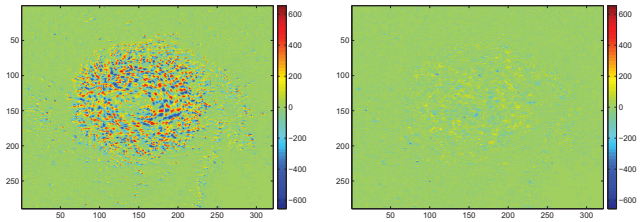

Fig. 3. Difference between image I_1 and image I_0 transported by: a constant null velocity field (initialization of the algorithm) on the left, the identified velocity field (after convergence of the algorithm) on the right, using the same scale.

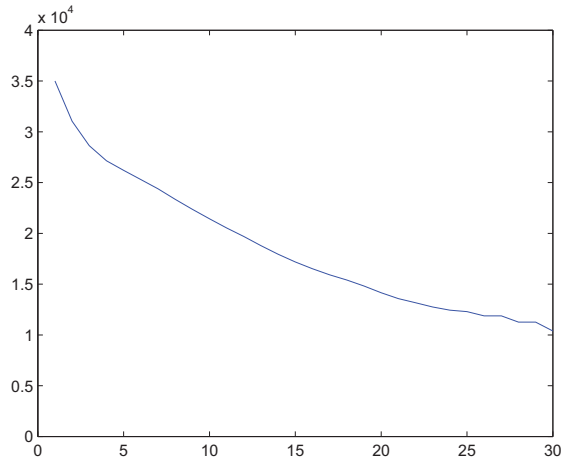

Fig. 4. Evolution of the cost function versus the number of iterations of the minimization process, with a multiscale approach: 24 iterations on the coarsest grid, respectively 3, 2 and 2 iterations on the intermediate grids, and 1 iteration on the finest grid.

Figure 4 shows the evolution of the cost function during the minimization process. Once again, it appears clearly that the global decrease of the cost function is done on the coarse grid, and it seems extremely efficient and fast to first identify the global structure of the velocity on the coarse grid, and then refine for details. The total computation time of this experiment is 7 minutes, nearly the computation time needed for 2 iterations on the finest grid.

We have compared the previous results with a non multiscale approach, on the same images, with the same numerical parameters. We have performed 10 iterations in the minimization process. We should recall that the identification process is done directly on the fine grid (1×1 pixel), and without any initial guess on the velocity field. Figure 5 shows the cor-

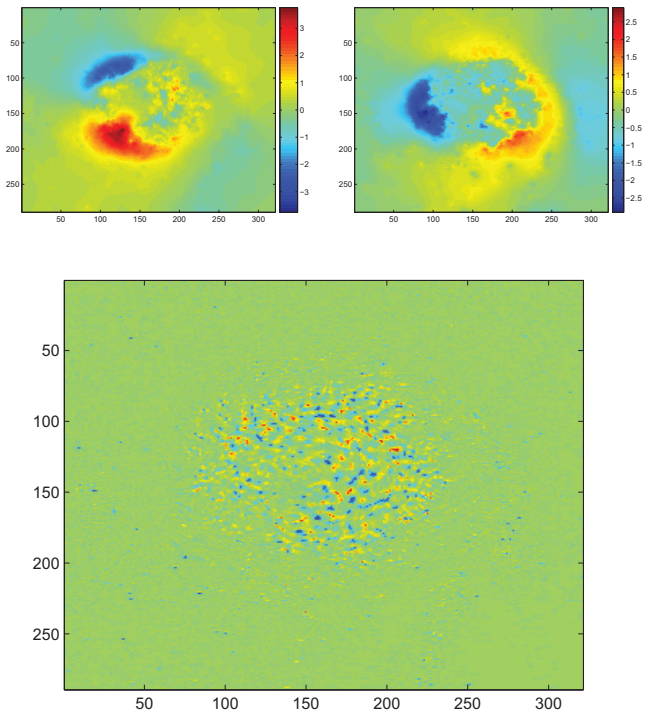

Fig. 5. Non multiscale approach for the identification of the velocity between images I_0 and I_1: longitudinal (top) and transversal (bottom) components of the velocity on the left, difference between image I_1 and image I_0 transported by this field.

responding results. On the left are represented the two components of the identified velocity after 10 iterations, and on the right the quality of the transport between the two images. Several conclusions can be drawn from this figure. Firstly, the computation time of this experiment was 33 minutes, more than four times the computation time of the previous multiscale approach. Secondly, the quality of the identified field is not good, as can be seen in figure 5 on the right (this figure should be compared with figure 3 on the right). The right part of the vortex has not been well transported. Moreover, the convergence of the algorithm was achieved after these 10 iterations, and the final value of the cost function is more than 1.5 times the final value in the multiscale approach. All these remarks clearly demonstrate the interest of a multiscale approach, both for regularizing the problem, and for a fast and effective estimation of the velocity field.

4. CONCLUSION

In this paper we presented an algorithm to estimate the motion between two images. This algorithm is based on the constant brightness assumption. A multiscale approach allows us to perform a minimization of the cost function in nested subspaces, the Jacobian matrix of the cost function being assembled rapidly at each scale using a finite element method. The coarse estimation allows one to avoid local minima, while the fine scales give more precise details. Several regularization terms are discussed, and it appears that the L^2 norm of the gradient gives reliable results.

The results of this algorithm on real fluid flows are presented, and they are encouraging both from their computational efficiency and from the quality of the estimated motion.

5. REFERENCES

[1] B. Horn and B. Schunk, "Determining optical flow," *Artifical Intelligence*, vol. 17, pp. 185–203, 1981.

[2] B. Lucas and T. Kanade, "An iterative image registration technique with an application to stereo vision," Vancouver, Canada, 1981, Proc Seventh International Joint Conference on Artificial Intelligence, pp. 674–679.

[3] P. Ananden, "A computational framework and an algorithm for the measurement of visual motion," *Int. J. Comput. Vis.*, vol. 2, pp. 283–310, 1989.

[4] S. Beauchemin and J. Barron, "The computation of optical flow," *ACM Computing Surveys*, vol. 27, no. 3, pp. 433–467, 1995.

[5] J. Fehrenbach and M. Masmoudi, "A fast algorithm for image registration," *C. R. Acad. Sci. Paris, Ser. I*, vol. 346, pp. 593–598, 2008.

[6] E. Mémin and P. Perez, "Optical flow estimation and object-based segmentation with robust techniques," *IEEE Trans. Image Proc.*, vol. 7, no. 5, pp. 703–719, 1998.

[7] P. Ruhnau, T. Kohlberger, C. Schnörr, and H. Nobach, "Variational optical flow estimation for particle image velocimetry," *Experiments in Fluids*, vol. 38, no. 1, pp. 21–32, 2005.

[8] T. Corpetti, E. Mémin, and P. Pérez, "Dense estimation of fluid flows," *IEEE Trans. Pattern Anal. Mach. Intel.*, vol. 24, pp. 365–380, 2002.

[9] A. Cuzol, P. Hellier, and E. Mémin, "A low dimensional fluid motion estimator," *Int. J. Comput. Vis.*, vol. 75, pp. 329–349, 2007.

[10] "Coriolis rotating platform," website `http://www.coriolis-legi.org/`.

[11] J. B. Flor and I. Eames, "Dynamics of monopolar vortices on the beta plane," *J. Fluid Mech.*, vol. 456, pp. 353–376, 2002.